

Liberation of slave modes inside domain walls in multiferroic Cu-Cl boracite

Peng Chen and Sergey Artyukhin

Quantum Materials Theory, Istituto Italiano di Tecnologia, 16163 Genova, Italy.

(Dated: March 14, 2024)

Domain walls (DWs), the two-dimensional boundaries between symmetry equivalent ferroic domains, are actively investigated due to their promise for novel logic and memory devices. Moreover, they can be easily created, erased and reshaped at a low energy cost due to their high mobility and large electrical conductivity. Most work so far has been focused on DWs in proper ferroelectrics, where the primary order parameter, ferroelectric polarization, interpolates between the values in the domains by either reducing to zero (in Ising-type DW) or rotating (Bloch type DW). Here we present a new member of DW family with a complex inner texture of slave order parameters inside the wall where the primary order parameter reduces to zero. Our first-principles-derived model predicts the existence of monopolar and toroidal polarization patterns. The results enable large-scale phase field simulations of complex domain patterns in boracites and could inspire novel devices based on domain walls in improper ferroelectrics.

Introduction. Boracites are among the first discovered multiferroic materials [1, 2], which however remain a source of puzzling experimental data. They are improper ferroelectrics, meaning that the polarization is induced through an anharmonic coupling with the primary order parameter, a 6-component X_5 mode, representing antipolar ionic displacements. The same antipolar distortion are also generally observed in the famous perovskite ground state structure $Pnma$. However, the X_5 modes are a secondary order parameters, slave to the in- and anti-phase rotation. The parent structure, $F\bar{4}3m$, is chiral, and therefore the components of electric polarization and shear strains transform according to the same irreducible representations, resulting in improper ferroelasticity. High dimension of the primary order parameter and strong interactions with the secondary ones gives rise to a rich free energy landscape with many domains, and complex domain patterns, observed in experiments. This explains the growing interest to boracites within the emerging field of domain wall-based nanodevice design [3]. Extensive work has also been done on magnetism in boracites, and the interplay between structural and magnetic orders [4, 5]. Presence of multiple interacting multicomponent orders positions boracites as an ideal playground for domain wall injection and manipulation [6].

In order to build a theoretical basis for understanding

of these puzzling phenomena, here we determine the parameters of a first-principles-based Landau-type theory, describing interacting antipolar displacements, ferroelectric polarization and strains in Cu-Cl boracite. Using the model, we simulate the domain wall structure and domain patterns.

Structure and Symmetry. Boracites are a crystal family with chemical formula $M_3B_7O_{13}X$, where M is a divalent metal and X is usually a halogen.

The parent structure is $F\bar{4}3c$, and at lower temperatures boracites undergo phase transitions driven by the dominant distortion modes X_5 and Γ_4 . At low temperatures Cu-Cl boracite adopts $Pca2_1$ structure. The group-subgroup analysis shows that the primary order parameter, corresponding to antipolar displacements, has six components $(a_1, a_2, b_1, b_2, c_1, c_2)$ and transforms according to the irreducible representation X_5 , while polarization and shear strains transform as Γ_4 . Components of X_5 with a, b, c describe modulations with wavevectors along a, b, c crystallographic directions. The distortions due to an antipolar mode c_1 and a polar mode P_3 are shown in Fig. 1. a_1 and b_1 modes are obtained by acting on c_1 with the 3-fold rotation around the body diagonal. P_1 and P_2 modes are obtained from P_3 analogously. $\bar{4}$ operation transforms between a_1 and a_2 etc. Only M and X

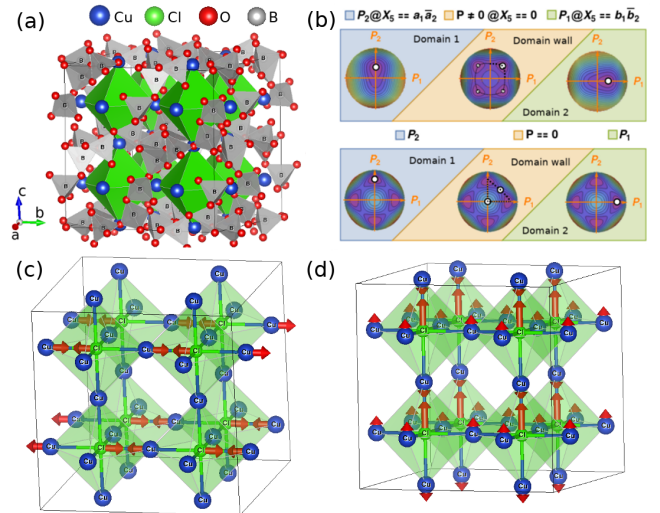


FIG. 1. (a) Boracite parent structure $F\bar{4}3c$; it can be separated into (b) perovskite structure of XM_3 octahedra and (c) and clusters of BO_4 tetrahedra at the A site of ABO_3 structure; (d) antipolar distortion mode c_1 ; (e) polarization mode P_3 .

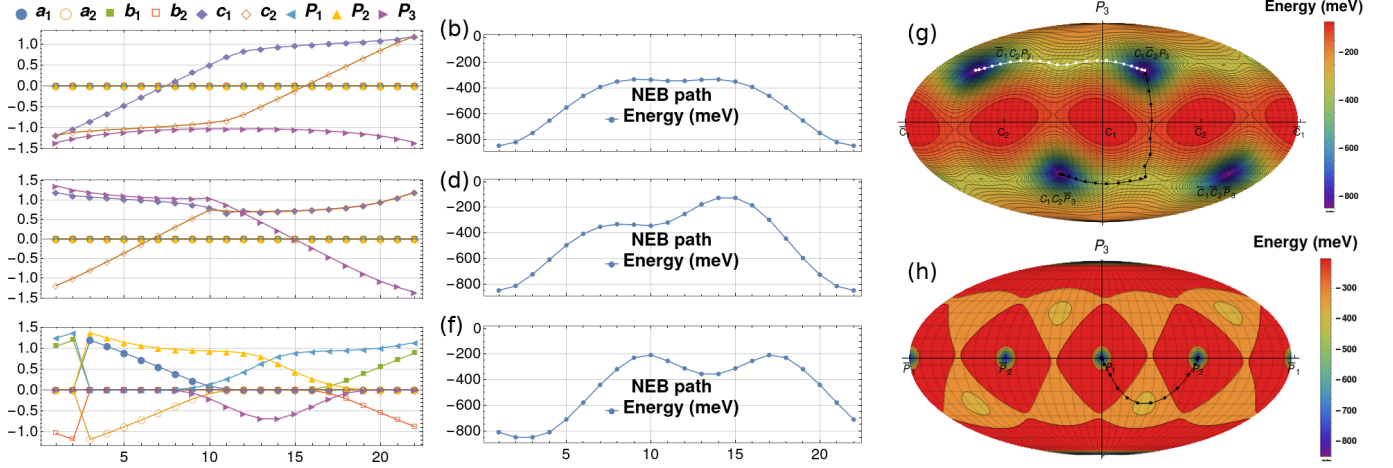


FIG. 2. A minimum energy path (MEP) from nudged elastic band (NEB) optimization. Energy along the MEP (a-c) and order parameters variations (d-f) across the domain wall between $\bar{c}_1\bar{c}_2\bar{P}_3$ and $c_1c_2\bar{P}_3$ in (a,d), $c_1\bar{c}_2P_3$ and $c_1c_2\bar{P}_3$ in (b,e), and $a_1\bar{a}_2P_2$ and $b_1\bar{b}_2P_1$ in (c,f); (g-h) Energy potential landscape on a Mollweide projection (see supplementary) with MEPs overlaid.

ions are shown in Fig. 1(d,e), as they contribute the most to the distortion, while the displacements of boron and oxygen ions are small. It is interesting that the boracite could be thought of as a simple perovskite structure ABO_3 with corner-sharing $ClCu_6$ octahedra, while the clusters of BO_4 tetrahedra substitute A cations, and break the inversion symmetry, present in perovskites. The absence of inversion symmetry in the parent structure of boracite allows exotic order parameter couplings, forbidden in typical perovskite-based ferroelectrics, such as $BaTiO_3$ and $BiFeO_3$. For example, boracite allows the coupling of polarization to X_5 modes, Eq. 3 $\gamma_{xp}P_3c_1c_2$, that gives rise to improper ferroelectricity, and a third order coupling among polarization components, Eq. 2 $\gamma_pP_1P_2P_3$. The complete list of invariants is presented in Table S2.

DFT energetics. To evaluate the interaction parameters of the model, we performed DFT total energy and phonon calculations on a number of representative low energy structures of Cu-Cl boracite, listed in Table S1. The ground state structure is 794.2 meV/8f.u. below the parent one. From the DFT energies presented in Table S1, we see that the structural chirality results in energy difference between the structures with the same (c_1, c_2) but opposite P_3 . Similarly, an energy difference could also be seen between $P_1P_2P_3$ and $\bar{P}_1\bar{P}_2\bar{P}_3$ phases and between $\bar{a}_1\bar{b}_1\bar{c}_1$ and $a_1b_1c_1$ phases. For the phase without X_5 and a ferroelectric polarization, the $a_2\bar{b}_2\bar{c}_2$ and $P_1P_2P_3$ are the low energy phases close to the ground state, which means that there is strong anisotropic coupling among Γ_4 polarization modes, and the same between X_5 antipolar displacement modes. Due to the coupling between Γ_4 polarization and X_5 antipolar displacements, the lowest energy state is the $c_1c_2\bar{P}_3$ phase. The coupling between X_5 antipolar displacement and Γ_4 shear strain does not significantly reduce the energy, $\Delta E = -32.6$ meV/8f.u., from c_1c_2 to c_1c_2e

phase. The Γ_4 polarization is another mode that couples to shear strain, and results in a similar energy gain, $\Delta E = -30.3$ meV/8f.u.

Extracting Landau model parameters. The coefficients are fitted from DFT and summarized in the Table S2. The negative γ_{xc} and positive γ_{xp} indicate that a positive primary order parameter c_1c_2 favours a positive shear strain and a negative polarization. However, the negative γ_{pc} tells that there is a strong competition between the positive shear strain and the negative polarization (induced by the same X_5 , c_1c_2). This interesting fact implies the competition between the two slave modes, the shear strain and polarization, due to the force from the master mode, X_5 antipolar displacements. While the coupling to X_5 forces the amplitudes of polarization and strain modes, frustrating their coupling to each other, these competing interactions in boracite could lead to a peculiar behavior at a phase transition or inside a domain wall, where the primary X_5 order disappears. In addition, this competition stabilizes the zero value of X_5 mode in the metastable rhombohedral state via the coupling between X_5 and Γ_4 . This is corroborated by the stable phonon spectrum in that state, shown in Fig. S1. For example, if an external electric field is opposite to the polarization in one region, the energy may still be gained on its interaction with the shear strain, leading to anomalous ferroelectric DW motion, where a domain with polarization opposite to the electric field grows. This possibility is unfortunately precluded in Cu-Cl boracite, where the piezoelectric tensor component d_{123} is not large enough. The negative coefficients (α_{xxXX} , α_{xyyy} , and α_{xxYY}) of anisotropic terms indicate that the components of X_5 attract to each other. In addition, there's a strong attractive interaction γ_x between a_1, b_1 and c_1 , which explains the very low energy of $\bar{a}_1\bar{b}_1\bar{c}_1$ phase in Table S1.

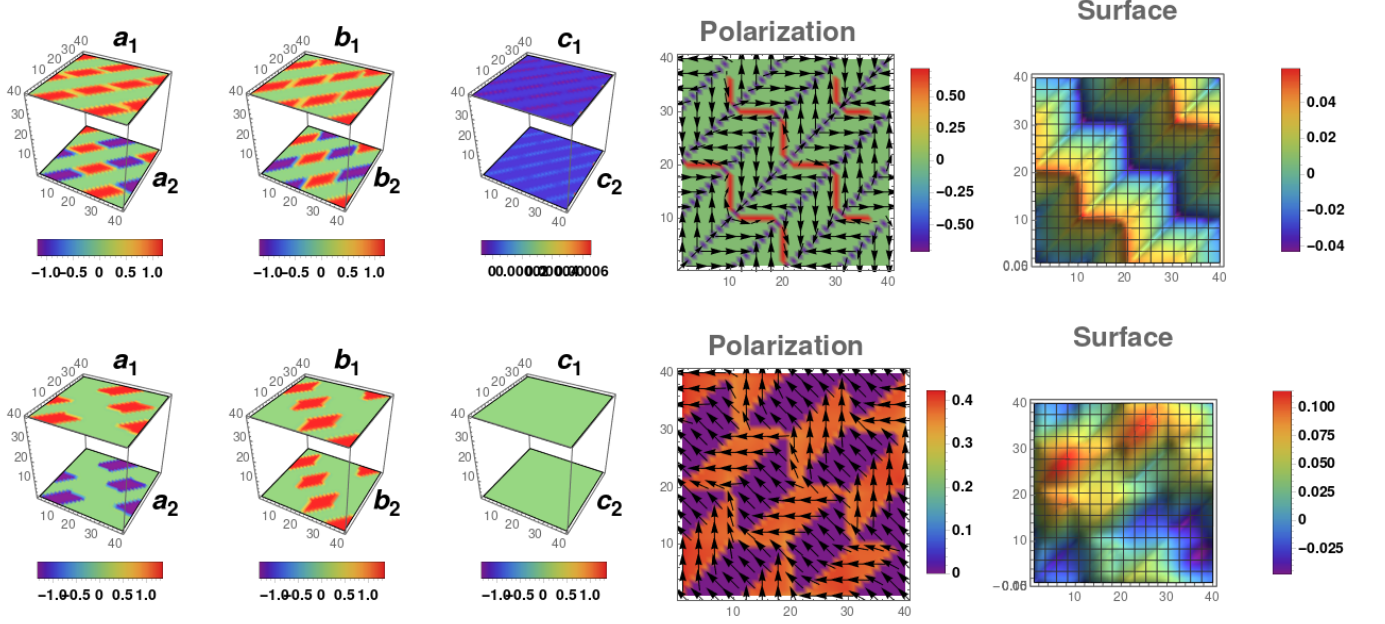


FIG. 3. The components of the X_5 mode for the Miura domain pattern with and without electric field. (a) $E = 0$, (b) $E = E_0$, (c) $E = 0$, (d) $E = E_0$; DW inside a DW is seen in panel (c) where the coloring of DW segments changes from yellow to blue. (e,f) Ferroelectric polarization texture corresponding to states represented in panels (a) and (d).

Domain walls in Cu-Cl boracite. Now we turn to the structure of domain walls in boracites. The nudged elastic band (NEB) method is utilized to explore the minimum energy paths (MEP) connecting different domains, corresponding to the minima on the potential energy surface in Eq. 1. Fig. 2(a, d) shows the energy barrier and the order parameter variation for the NEB between $\bar{c}_1\bar{c}_2\bar{P}_3$ and $c_1c_2\bar{P}_3$ domains. The corresponding MEP is marked with a white curve in Fig. 2(g). Ferroelectric polarization does not change sign across the wall, and hardly changes along the path (Fig. 2(d)), hence we call this 0° DW. The intermediate phase is a metastable local minimum $c_1\bar{c}_2\bar{P}_3$ (see Supplementary section ???).

As for the DW between $c_1\bar{c}_2P_3$ and $c_1c_2\bar{P}_3$ phases, where polarization is reversed (180° ferroelectric DW), the MEP, shown with the black curve in Fig. 2(g), is asymmetric. MEP passes through a local minimum $c_1\bar{c}_2\bar{P}_3$ and a saddle point $c_1\bar{c}_2$. Note that an equivalent MEP through c_1c_2 and $c_1c_2P_3$ exists, potentially allowing to use an electric field to drive a hysteretic switching between the two. Under an external electric field, a segment of c_1c_2 wall will nucleate inside the $c_1\bar{c}_2\bar{P}_3$ wall, and the boundary between them would represent a 1D topological defect, that appears naturally in our simulations, e.g. shown in Fig. 3. Fig. 2(e) indicates that this is an Ising-type ferroelectric DW, so that P_3 changes, while other polarization components are zero.

The most interesting is the ferroelectric 90° DW, whose MEP is shown in Fig. 2(h). It has a symmetric barrier. Surprisingly, the intermediate rhombohedral phase

is $P_1P_2\bar{P}_3$, seen in Fig. 2(f), with $P_1 = P_2 = P_3$. Along the path, the X_5 components $a_1\bar{a}_2$ reduce to zero, however, the $b_1\bar{b}_2$ does not increase until the intermediate phase is reached (fig. 2(h)). Note that the primary order parameter is X_5 , and the polarization is a slave order. When X_5 is present, the double well potential for the polarization is highly tilted, which is illustrated by contour plots inside domains in Fig. 1(c). However, the NEB optimization indicates that X_5 is zero inside the 90° DW and, surprisingly, the slave polarization modes are liberated and become the primary modes inside the wall, which gives the DW a complex inner structure.

To the best of our knowledge, this special type of DW has never been reported, although it plays a key role in the formation of DW patterns and in DW motion discussed in the following section.

Miura patterns, monopolar and ferro-rotational polarization configurations.

Paper can be folded into a famous Miura pattern, seen in Fig. 3, that conserves the area of the sheet. Similarly, $\epsilon_{xz}, \epsilon_{yz}$ strains in boracite tilt its surface but do not change its area, and therefore boracite domain adopt this pattern, since assembly of such sheared unit cells does not result in external surface tension. In the Miura domain pattern, the vertical and horizontal DWs are 180° and all the diagonal DWs are 90° walls. As we see, DWs are in a rhombohedral phase, $P_1 = P_2 = P_3$. When the electric field is applied, the domains with polarization along the field remain, while the domains with antiparallel polarization are converted into the rhombohe-

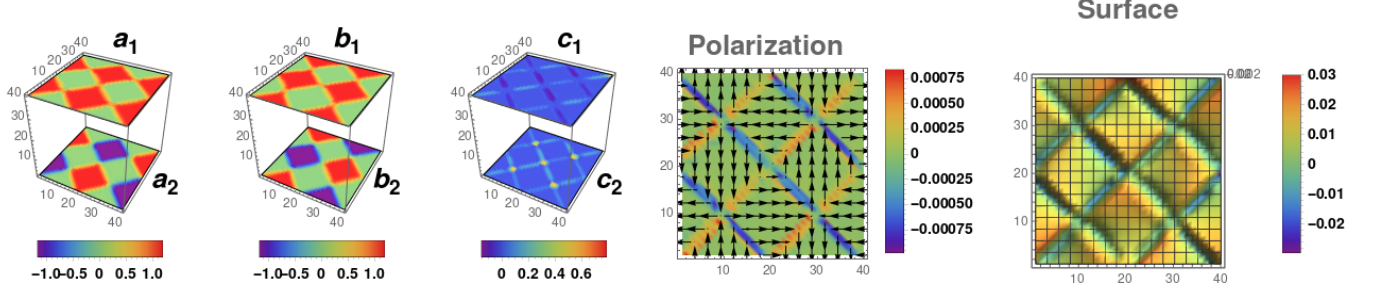


FIG. 4. Miura, toroidal and ferrorotational polarization patterns in boracites.

dral $P_1 = P_2 = P_3$ phase. This suggests that domains in the Miura pattern with polarization along the field are protected, while others could be altered. Notably, the in-plane electric field here induces out-plane polarization and current. These exotic phase transformations under electric field could be utilized to implement memory read and write operations. Taking advantage of the 90°

DWs, ferro-rotational and monopolar polarization patterns, shown in Fig. 4 could also be injected in boracites via an application of a mechanical force.

Methods. The parameters of the Ginzburg-Landau model are extracted by fitting the total energies and phonon dispersion from first principle calculations to the model free energy,

$$f = f_x + f_p + f_c + f_{xp} + f_{xc} + f_{pc} + G_X \nabla_i X_j \nabla_i X_j + G_P \nabla_i P_j \nabla_i P_j, \quad (1)$$

$$f_x = \alpha_i X_i^2 + \alpha_{ij} X_i^2 X_j^2 + \alpha_{ijk} X_i^2 X_j^2 X_k^2 + \gamma_x (a_1 b_1 c_1 - a_2 b_2 c_2),$$

$$f_p = \beta_i P_i^2 + \beta_{ij} P_i^2 P_j^2 + \beta_{ijk} P_i^2 P_j^2 P_k^2 + \gamma_p P_1 P_2 P_3, \quad (2)$$

$$f_c = \frac{1}{2} \epsilon_{ij} C_{ijkl} \epsilon_{kl} + \gamma_c \epsilon_{13} \epsilon_{23} \epsilon_{12},$$

$$f_{xp} = \gamma_{xp} (a_1 a_2 P_2 + b_1 b_2 P_1 + c_1 c_2 P_3) + \eta_{xp} ((a_1 b_2 c_1 - a_2 b_1 c_2) P_1 + (a_2 b_1 c_1 - a_1 b_2 c_2) P_2 + (a_1 b_1 c_2 - a_2 b_2 c_1) P_3), \quad (3)$$

$$f_{xc} = \gamma_{xc} (a_1 a_2 \epsilon_{13} + b_1 b_2 \epsilon_{23} + c_1 c_2 \epsilon_{12}) + \eta_{xc} ((a_1 b_2 c_1 - a_2 b_1 c_2) \epsilon_{23} + (a_2 b_1 c_1 - a_1 b_2 c_2) \epsilon_{13} + (a_1 b_1 c_2 - a_2 b_2 c_1) \epsilon_{12}),$$

$$f_{pc} = -\frac{1}{2} q_{ijkl} \epsilon_{ij} P_k P_l + \gamma_{pc} (P_2 \epsilon_{13} + P_1 \epsilon_{23} + P_3 \epsilon_{12}),$$

where the distortion modes $X_5 (a_1, a_2, b_1, b_2, c_2, c_1)$, polarization (P_1, P_2, P_3) , and unit cell displacements (u_1, u_2, u_3) , related to strain components via $\epsilon_{ij} = \frac{1}{2}(\partial_j u_i + \partial_i u_j)$, are identified by group-subgroup analysis. The gradient terms in (1) penalize spatial variations of order parameters. f_x and f_p represent Mexican hat-like potentials for X_5 and P modes; f_c stands for the elastic energy, while f_{xp} and f_{xc} describe interactions between X_5 modes and ferroelectric polarizations and strains, respectively. f_{pc} accounts for the energy due to electrostriction and a piezoelectric effect. Note that we have neglected $\gamma_c \epsilon_{23} \epsilon_{13} \epsilon_{12}$ term. Although γ_c drives instability of shear strains, calculations suggest the associated strain amplitude to be only 1/100 of the ground state shear strain, and therefore we drop this term.

Density functional theory calculations [7, 8] are performed using VASP code [9], with projector-augmented wave formalism [10, 11] and PBEsol exchange-correlation functional [12]. The total energy calculations are performed with 500 eV energy cutoff and Monkhorst-Pack

3x3x3 k-mesh [13]. We use 192-atom supercells compatible with all the distortions discussed in this study. The representative structures were chosen in the following way. The symmetry inequivalent combinations of X_5 antipolar and Γ_4 polarization modes are frozen into the cubic structure and geometric optimization was performed to obtain all the structures, corresponding to all the energy minima and saddle points. The energies of those states and some others are reported in Table S1. Then the training sets for model fitting [14] are generated by varying mode amplitudes with constant increments around each individual minimum and saddle point, until the energy change of tens of meV is reached.

The elastic moduli and interatomic force constants are calculated using density functional perturbation theory [15]. Phonopy package [16] is used in the phonon spectrum calculations. Minimum energy paths were determined with the help of the nudged elastic band method [17] which can give the most energetically favorable intermediate configuration between the initial and final struc-

tures.

-
- [1] E. Ascher, S. H., and D. Tar, Solid State Communications **2**, 45 (1964).
 - [2] E. Ascher, H. Rieder, H. Schmid, and H. Stssel, Journal of Applied Physics **37**, 1404 (1966).
 - [3] G. Catalan, J. Seidel, R. Ramesh, and J. F. Scott, Rev. Mod. Phys. **84**, 119 (2012).
 - [4] P. Tolédano, H. Schmid, M. Clin, and J. P. Rivera, Japanese Journal of Applied Physics **24**, 179 (1985).
 - [5] J. Feng, K. Xu, L. Bellaiche, and H. Xiang, New Journal of Physics **20**, 053025 (2018).
 - [6] R. G. P. McQuaid, M. P. Campbell, R. W. Whatmore, A. Kumar, and J. M. Gregg, Nature Communications **8**, 15105 (2017).
 - [7] P. Hohenberg and W. Kohn, Phys. Rev. **136**, B864 (1964).
 - [8] W. Kohn and L. J. Sham, Phys. Rev. **140**, A1133 (1965).
 - [9] G. Kresse and J. Furthmüller, Phys. Rev. B **54**, 11169 (1996).
 - [10] P. E. Blöchl, Phys. Rev. B **50**, 17953 (1994).
 - [11] G. Kresse and D. Joubert, Phys. Rev. B **59**, 1758 (1999).
 - [12] J. P. Perdew, A. Ruzsinszky, G. I. Csonka, O. A. Vydrov, G. E. Scuseria, L. A. Constantin, X. Zhou, and K. Burke, Phys. Rev. Lett. **100**, 136406 (2008).
 - [13] H. J. Monkhorst and J. D. Pack, Physical Review B **13**, 5188 (1976).
 - [14] P. Chen and S. Artyukhin, “Landau model builder,” <https://github.com/PaulChern/L-INVARIANTS> (2019).
 - [15] S. Baroni, S. de Gironcoli, A. Dal Corso, and P. Gianozzi, Rev. Mod. Phys. **73**, 515 (2001).
 - [16] A. Togo and I. Tanaka, Scripta Materialia **108**, 1 (2015).
 - [17] G. Mills, H. Jónsson, and G. K. Schenter, Surface Science **324**, 305 (1995).